Effect of a serrated skirt on the buffeting phenomenon in transonic afterbody flows

Philippe MELIGA, Philippe REIJASSE and Jean-Marc CHOMAZ
ONERA, Fundamental and Experimental Aerodynamics Department
8 rue des Vertugadins, 92190 Meudon, France
philippe.meliga@onera.fr

Abstract. The transonic flow past an axisymmetric afterbody equipped with a propulsive nozzle is investigated experimentally through wall-pressure measurements. The length of the nozzle is chosen so that the flow reattaches on the external nozzle wall. In the subsonic regime, the spectra in the separated region exhibit a well-defined periodicity corresponding to the shedding of large-scale structures in the wake, associated with a highly coherent m=1 mode. Near the reattachment point, the spectra exhibit high intensity fluctuations due to the shear layer vortices impinging the downstream surface. In the low supersonic regime, the pressure fluctuations are decorrelated and the spectra in the separated region are similar to those obtained in the upstream boundary layer. A reduction of pressure and side loads fluctuations is achieved by use of a short serrated skirt that induces a downstream displacement of the reattachment point. However, we find no effect of the teeth on the spatial organisation of the separated area.

Key words: afterbody flow, transonic, unsteadiness, buffeting, side loads, reduction device.

1. Introduction

Launcher afterbody flows are characterized by a massive separation occurring at the base region due to an abrupt change in the rear geometry. The unsteadiness of the separated flow generates strong low frequency wall-pressure fluctuations and induces aerodynamic excitation. The resulting high dynamic loads can excite a response of the structural modes termed buffeting that can be critical during the transonic phase of flight, as experienced by the Ariane V launcher.

The base pressure properties of separated flows have been experimentally and theoretically studied in the last decades [6, 8, 12, 13]. For complex afterbody shapes [1, 2, 4], several aerodynamics phenomena are simultaneously at work (recirculating area, reattachment of the separated shear layer on a solid surface, acoustic radiation of the propulsive jet), and limit the knowledge of the separated dynamics. Reducing the pressure fluctuations level hence remains a challenge to improve the performances and the reliability of the future launch vehicles.

A study by Deprés et al. [3, 5] has enlightened the wall-pressure properties of axisymmetric blunt configurations equipped with a cylindrical rear-body of variable length. The main idea developped in this study is that despite the broad variety of control parameters, two main kinds of separation are to be considered, depending on whether the separated external flow does or does not reattach on

the rear-body. For short rear-bodies, the flow organisation is dominated by the periodic shedding of large scale structures, as observed for bluff bodies, as shown by the far wake velocity measurements of Flodrops and Desse [7]. For sufficiently long rear-bodies, the unsteady dynamics is dominated by the reattachment process of the separated shear layer (see the review of Mabey [9]). The high intensity fluctuations can then be ascribed to the shear layer vortices impinging the downstream surface. A possible solution to reduce the flow unsteadiness is to prevent the reattachment of the shear layer. Among the different existing solutions, the use of skirts, whose effect is to displace downstream the separation point of the incoming boundary layer, has been proven efficient, although the reduction achieved remains weak compared to the fluctuations levels. This paper presents an experimental investigation of a long rear-body configuration based on wall-pressure measurements. We aim at assessing the efficiency of a short serrated skirt to reduce the unsteady activity to which the base region is submitted. Teeth susceptible to promote the small-scale turbulence are expected to affect significantly the spatial organization of the flow and to enhance the effect of a classical skirt. We also consider the case of a low supersonic upstream flow with no reduction device.

2. Description of the study

Tests are carried out in the S3Ch continuous transonic wind tunnel of ONERA. The afterbody is made of an axisymmetric blunt-based body of diameter D = 100mm equipped with a rear-body, whose exit plane is located at a distance L = 120mm downstream of the base. The external nozzle surface is a cylindrical body of diameter d = 40mm (Figure 1a). This geometry was chosen because the aspect ratio L/D = 1.2 allows for a reattachment of the separated shear layer near the end of the rear-body, and because it allows comparison, in the range of Mach numbers $0.7 < M < 0.85$, with the experimental data of Deprés et al. [5]. The serrated skirt is made up of 12 teeth of length 33 mm (Figure 1b). Steady and unsteady wall-pressure measurements are performed using 77 pressure taps mounted on the cylindrical forebody, the base area, and the rear-body region, both in the streamwise and azimuthal directions. Time histories of the unsteady pressures are recorded over 12 seconds. The static component is measured using 12 Statham sensors, and the fluctuating component is recorded simultaneously using 65 Kulite sensors, at a sampling rate of 10240 Hz.

The models are mounted at the end of a cylindrical forebody fixed in the wind-tunnel settling chamber, and all tests are performed at zero incidence. The no-skirt configuration, herein referred to as the nominal configuration, is investigated for free stream Mach numbers M = 0.7, 0.9 and 1.3. The skirt configuration is tested at M = 0.7. The initial external boundary layer grows on the upstream cylindrical sting over a distance of over 10D before reaching the base corner. Because the set up of the Mach and Reynolds numbers could not be

done independently, the Reynolds number based on the forebody diameter D varies from $1.35 * 10^6$ at M = 0.7 to $2.60 * 10^6$ at M = 1.3. The effect of a propulsive jet at adaptation is also investigated. In this analysis, we discuss only the no jet configurations, as no significant effect of the jet was found, due to the limited interaction between the afterbody and the jet shear layers. Unless specified, all results pertain to the sensors in the azimuthal plane $\theta = 0°$.

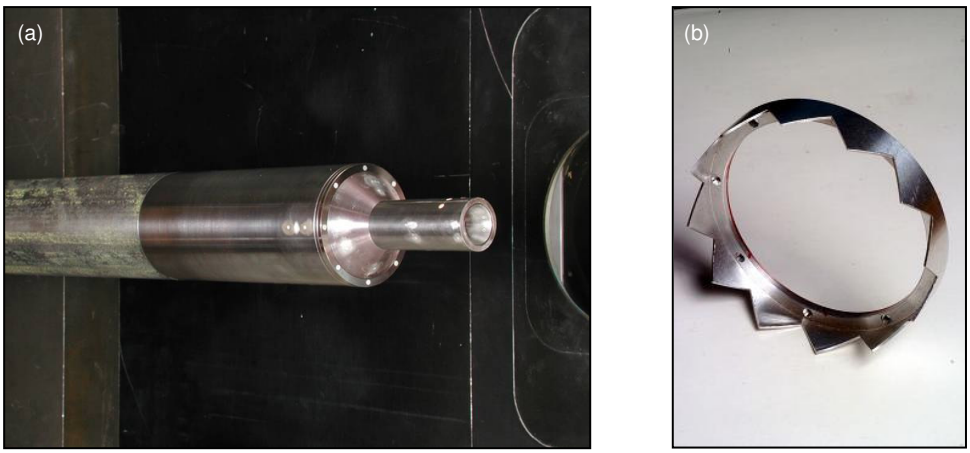

Figure 1. (a): Nominal configuration in the S3Ch wind tunnel. (b): Detail of the serrated skirt.

3. Results

3.1. STATIC AND FLUCTUATING PRESSURE DISTRIBUTIONS

In the following, we use the non-dimensional C_p and C_{prms} coefficients built on the free stream dynamic pressure q_∞, respectively defined as

$$C_p = (p-p_\infty)/q_\infty \qquad C_{prms} = \langle p'^2 \rangle^{1/2}/q_\infty \qquad (1)$$

Figures 2a and 2b show the streamwise distributions of C_P and C_{Prms} of the nominal configuration. The C_P data corresponding to previous experiments carried out by Maury [11] in the same wind tunnel for a long rear-body of ratio L/D = 9 are provided for comparison (grey diamond symbols), and confirm that the rear-geometry is seen as an axisymmetric backward facing step. The pressure measurements upstream of the base (x/D < 0) show a loss of influence of the recirculating area on the incoming boundary layer as the Mach number reaches supersonic values. Hence, the static pressure is lower than p_∞ for M = 0.7 and 0.9 (C_P = -0.06 at x/D = -0.4) increases dramatically until it becomes greater than p_∞ for M = 1.3 (C_P = 0.08). The base pressure is C_P = -1.16 for M = 0.7 and 0.9 and C_P = -1.17 at M = 1.3. These values are in excellent agreement with that reported by Deprés et al. [5] at M = 0.85 (C_P = -1.17). The streamwise distribution of C_P mainly follows two stages, with a slight decrease in the separated area up to x/D ~ 0.6, followed by a strong recompression. The maximum pressure is

obtained at the end of the rear-body where $p > p_\infty$. The C_{Prms} distribution increases with the streamwise position. For M = 0.7, the pressure fluctuations reach a maximum at x/D ~ 1, where they represent 4% of the upstream dynamic pressure, and then level off. This is characteristic of the shear layer reattachment that occurs at the extremity of the rear-body [5, 9].

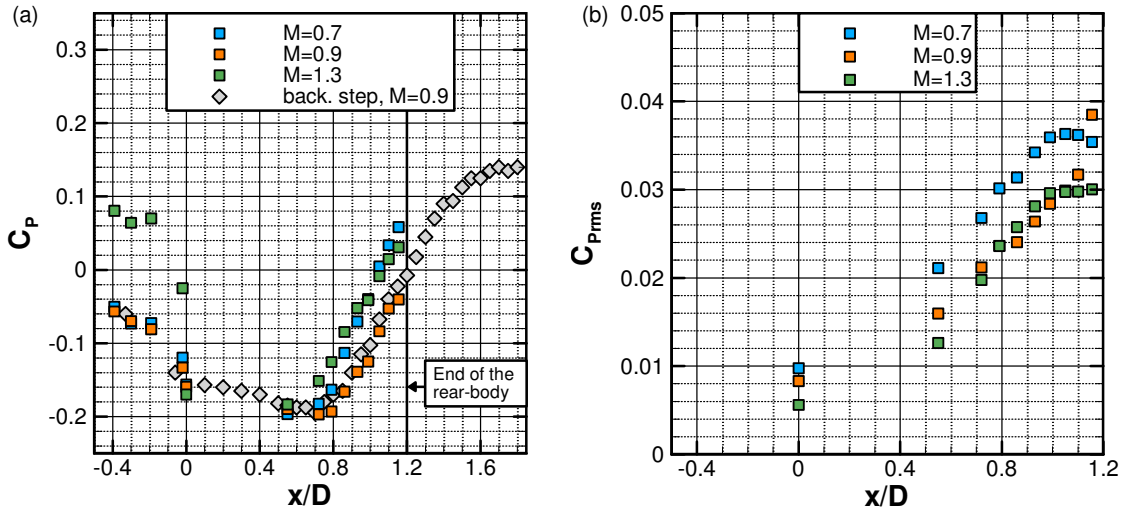

Figure 2. (a): Streamwise distributions of static pressure for the nominal configuration and for previous experiments carried out for a backward facing step configuration at M = 0.9. The vertical thick line at x/D=1.2 corresponds to the effective end of the rear-body in the configuration investigated. The yellow symbols correspond to static pressure levels measured by the Statham sensors. (b): Streamwise distributions of the pressure fluctuations.

The increase of the Mach number, up to 0.9, results in a decrease of the static pressure in the recompression area, and of the fluctuation levels in the whole separation. The shift downstream of the recompression point from x/D = 0.7 to x/D = 0.8, as well as the absence of plateau in the C_{Prms} distribution (the maximum being obtained at the end of the rear-body), are probably linked to the reattachment length with the Mach number in the subsonic regime [9]. This is confirmed by the instantaneous schlieren photograph (Figure 3a): the shape of the shear layer external envelope suggests that the shear layer does not fully reattach, a result consistent with the reattachment length equal to 1.4 obtained by Maury [11] at this Mach number, which is larger than the rear-body extension. The reattachment of the shear layer hence accounts for the high intensity of pressure fluctuations measured in the recirculating area. When the Mach number is further increased, up to 1.3, the recompression point shifts upstream from x/D = 0.8 to x/D = 0.65. For x/D > 1, the plateau reappears in the C_{Prms} distribution, suggesting that the reattachment length has shortened, so that the external flow does reattach again on the rear-body. This reattachment is the consequence of the expansion waves arising at the base corner for this supersonic upstream flow, which focus the shear layer towards the symmetry axis, and is visible on the schlieren photograph (Figure 3b). No significant effect of the

supersonic regime on the normalized fluctuation levels is found, and the levels in the separated region remain comparable to that measured for M = 0.9.

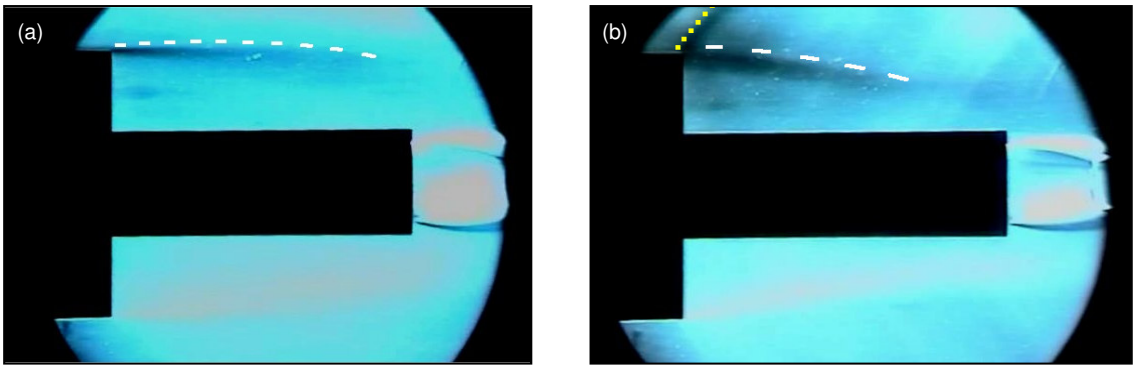

Figure 3. Schlieren photographs of the nominal configuration. The dashed thick line corresponds to the external envelope of the separated shear layer (a): M = 0.9. (b): M = 1.3. The dotted line corresponds to the expansion waves arising at the base corner.

By comparison with the nominal configuration at M = 0.7, the addition of a serrated skirt results in a negligible increase of the base pressure ($\Delta C_P \sim 0.02$ for $x/D < 0.7$, see Figure 4a), but the beginning of recompression process is shifted downstream from x/D = 0.7 to x/D = 0.8, thus leading to smaller static pressures ($\Delta C_P \sim 0.05$) on the final part of the rear-body. It also induces a small decrease of the fluctuation levels ($\Delta C_{Prms} \sim 0.006$ on the whole rear-body, corresponding to a reduction of ~ 2%, see Figure 4b) and the plateau disappears, as the maximum fluctuation level is now reached at the end of the rear-body. This general downstream shift can be fully ascribed to the displacement of the separation point of the boundary layer, from the base corner to the skirt averaged end, that prevents the shear layer from reattaching at the end of the rear-body.

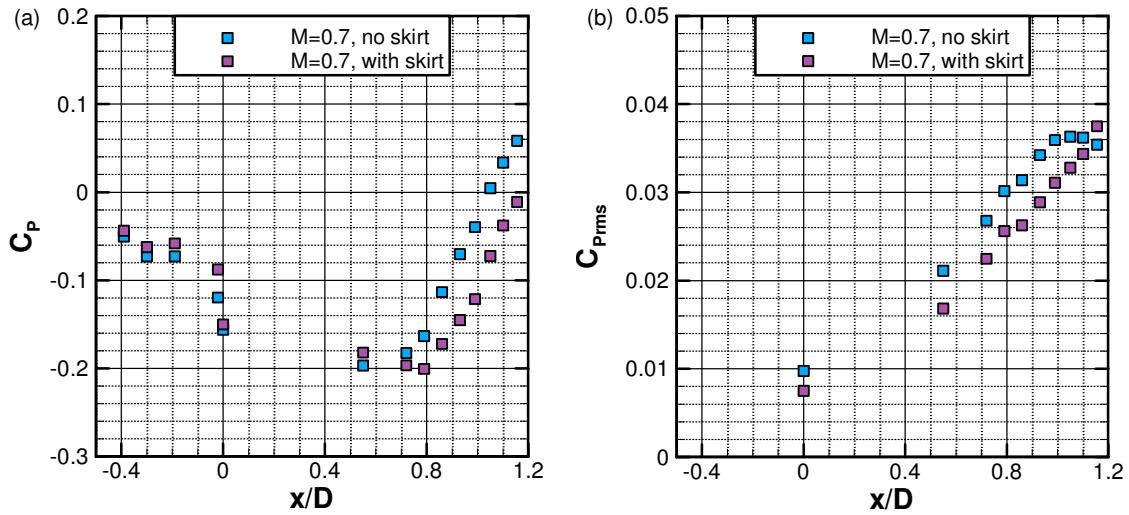

Figure 4. Comparison of the nominal and the skirt configurations at M = 0.7. (a): Static pressure distributions. (b): Pressure fluctuations distributions.

3.2. POWER DENSITY SPECTRA AND COHERENCE ANALYSIS

Wall-pressure spectra are investigated in order to identify the most energetic frequencies involved in the flow unsteadiness. Results are given in terms of the auto-correlation fuction S_{xx} and the Strouhal number St defined as

$$St = fL/U_\infty \tag{2}$$

Cross-correlations are also investigated for circumferencial sensor distributions located at a given streamwise position. Considering the cross-correlation function S_{xy} between two sensors x and y, S_{xx} and S_{yy} being the respective auto-correlation functions, we investigate the normalized cross-correlation function C and its Fourier decomposition in azimuthal modes, defined as

$$C(St, \Delta\theta) = S_{xy}(St, \Delta\theta) / [S_{xx}(St).\, S_{yy}(St)]^{1/2} \tag{3}$$
$$C(St, \Delta\theta) = \Sigma\, C_m(St) e^{im\Delta\theta} \tag{4}$$

Results are then provided in terms of the coherence function $\gamma = |C|$ and of the azimuthal coherence function $\gamma_m = |C_m|$, which can be seen as the percentage of fluctuating energy relative to the m^{th} azimuthal mode at a given frequency.

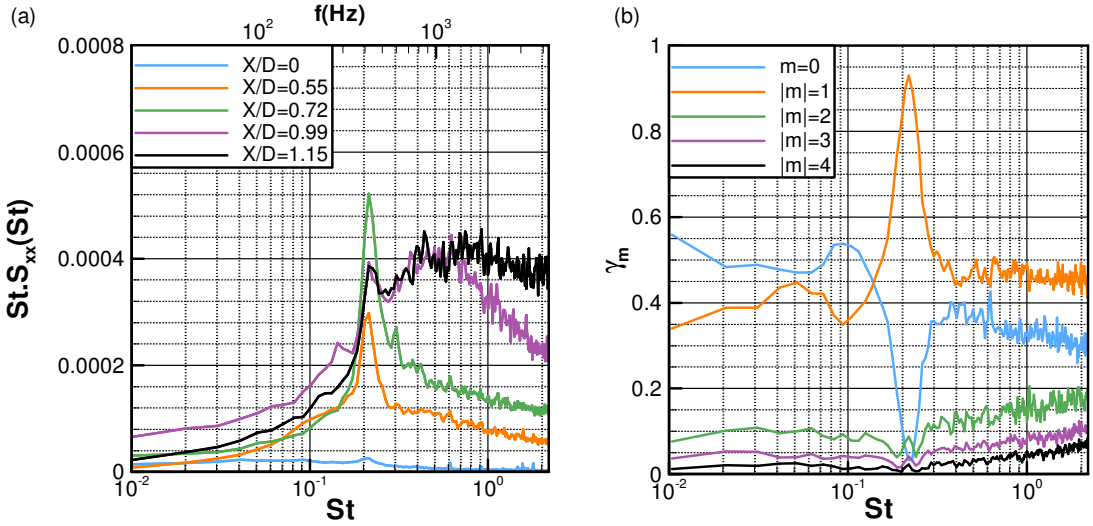

Figure 5. Nominal configuration at M=0.7. (a): Pressure spectra on the rear-body. (b): Coherence spectra of the first five azimuthal modes.

Figure 5a shows the power density spectra of the nominal configuration at M = 0.7. At the base, the spectra are dominated by a broad maximum at St ~ 0.1, corresponding to the flapping of the shear layer. Further downstream (x/D = 0.55 and 0.72), the spectra exhibit a narrow peak at the frequency St ~ 0.22, which is the signature of the low frequency shedding of large scale turbulent vortices, as observed in the context of bluff bodies. In their experimental study based on velocity measurements, Flodrops and Desse [7] have identified this phenomenon

in the far wake of an axisymmetric blunt based body (but not in the near wake), the corresponding Strouhal number being St ~ 0.21 at M = 0.85. The increase of pressure-fluctuations observed in the reattachment zone results from broadband energy frequencies of magnitude three to four times larger than the vortex shedding frequency, and corresponds to shear layer vortices impinging the rear-body surface. Figure 5b presents the coherence spectra for the modes of azimuthal wavenumbers $|m| < 4$ at $x/D = 0.72$, i.e. the azimuthal Fourier decomposition of the complex coherence function as a function of the frequency. The vortex shedding phenomenon found from the spectra is due to the existence of a highly coherent mode of azimuthal wavenumber $m = 1$, whose energy represents ~ 85% of the pressure fluctuations measured at this frequency at this particular downstream station inside the recirculation zone. This strongly suggests that a global coherent mode of azimuthal wavenumber $m = 1$, beating at the vortex shedding frequency, arises from the recirculating area.

For M=1.3, the separated zone exhibits no particular frequency (Figure 6a), and no particular azimuthal structure. Figure 6b hence shows that the correlation between the signals recorded by sensors located at the same downstream station decreases dramatically for all frequencies as the angular distance between sensors increases. This behaviour, typical of fully turbulent flows, indicates that the previous coherent global mode does not develop anymore in the near wake.

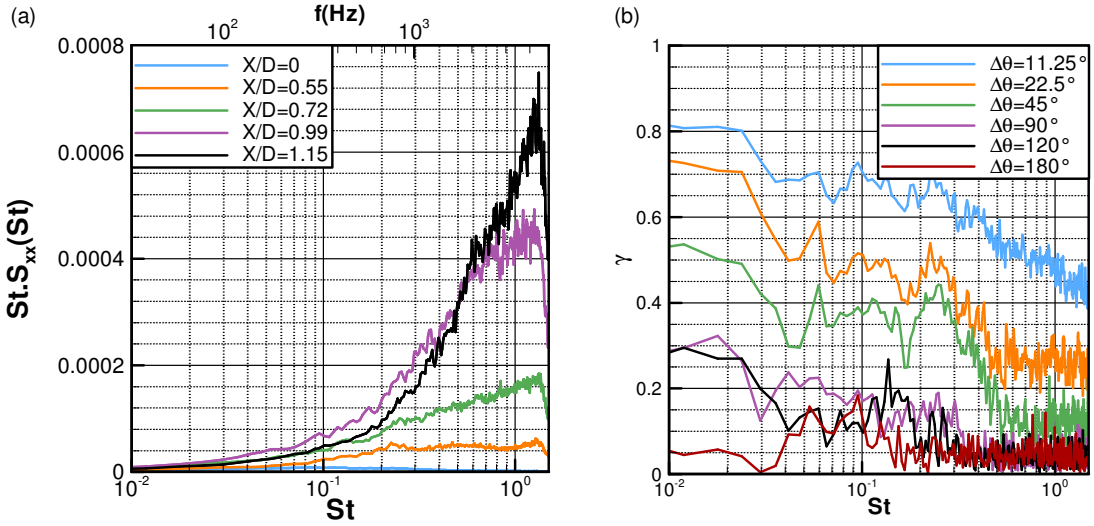

Figure 6. Nominal configuration at M=1.3. (a): Pressure spectra on the rear-body. (b): Coherence function for various angular distances.

The case of the skirt configuration at M = 0.7 is presented on Figures 7a and 7b. The pressure spectra (Figure 7a) exhibit the same predominant ranges of frequencies, associated to the same aerodynamical unsteady mechanism, namely the shear layer flapping at the base, the vortex shedding phenomenon at $x/D = 0.72$ and the shear layer reattachment at the end of the rear-body. The decrease of the fluctuation levels is related to a lower level of the broadband high frequency component, for $x/D < 1$, whereas no significant effect is found at

x/D = 1.15. In return, we find a higher contribution of the peak associated to the vortex shedding phenomenon, even at the end of the rear-body. This is confirmed by the azimuthal coherence analysis (Figure 7b), which shows that the m=1 coherent global mode still develops in the near wake and that its intensity increases slightly, as it represents ~ 95% of the pressure-fluctuations at the vortex shedding frequency. The skirt therefore acts as a smooth short skirt. In particular, the presence of teeth does not affect the spatial organization of the flow.

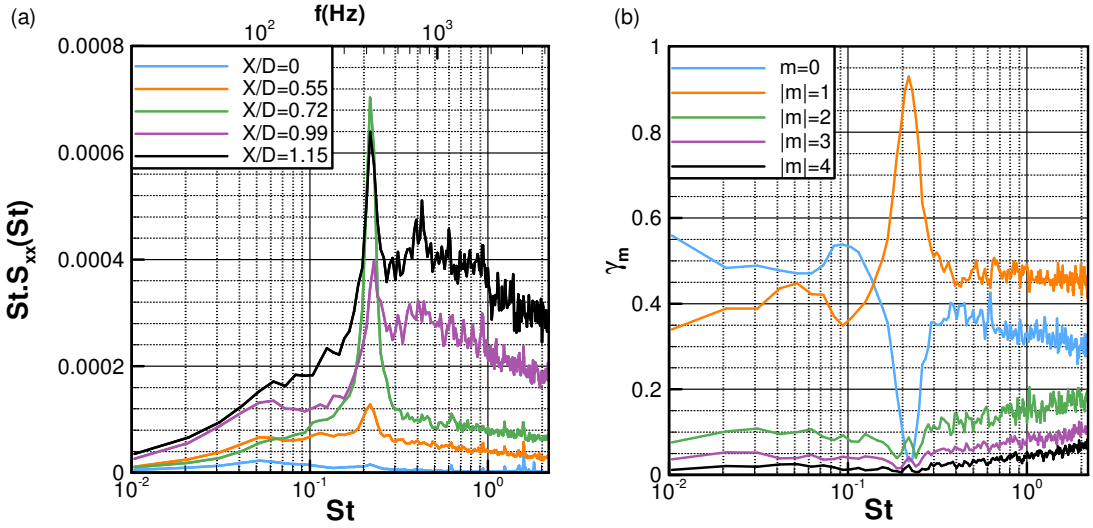

Figure 7. Skirt configuration at M=0.7. (a): Pressure spectra on the rear-body. (b): Coherence spectra of the first five azimuthal modes.

3.3. ESTIMATION OF THE UNSTEADY SIDE LOADS

In this section, the *x*- and *y*- axis are chosen respectively parallel to the θ=0° and θ=90° directions and orthogonal to the streamwise direction. Streamwise densities of the unsteady side loads resulting from the fluctuating wall-pressure field are computed in the *x*- and *y*- directions by integrating the wall-pressure field over the rear-body circumference. All side loads are then normalized with respect to the upstream dynamic pressure and external surface of the rear-body. Results are provided in terms of the side loads coefficients CF_x and CF_y.

Figure 8 shows the time series of the the side loads coefficients for the nominal configuration (x/D=0.72, M=0.7). We obtain a random signal (note that no privileged direction arises from Figure 8), that we investigate statistically. We restrict here to the spectra of the *y*- component CF_y. Figures 9a and 9b present the spectra of the side loads coefficients for the nominal and the skirt configurations at M=0.7. Similar to the case of wall-pressure fluctuations, the spectra are dominated by the vortex shedding process at x/D=0.72 and by the shear layer reattachment at x/D=1.15. As shown by the pressure measurements analysis, the use of the serrated skirt leads to a noticeable decrease of the side loads at x/D=0.72, but the effect in the reattachment area is negligible.

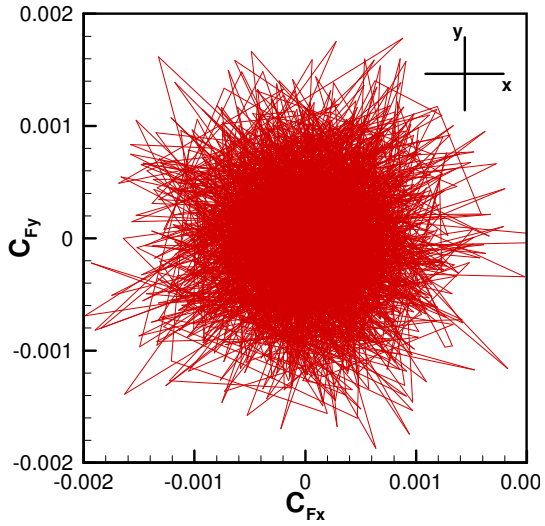

Figure 8. Time series of the normalized side load density in the (CFx, CFy)-plane (nominal configuration, M=0.7, x/D=0.72)

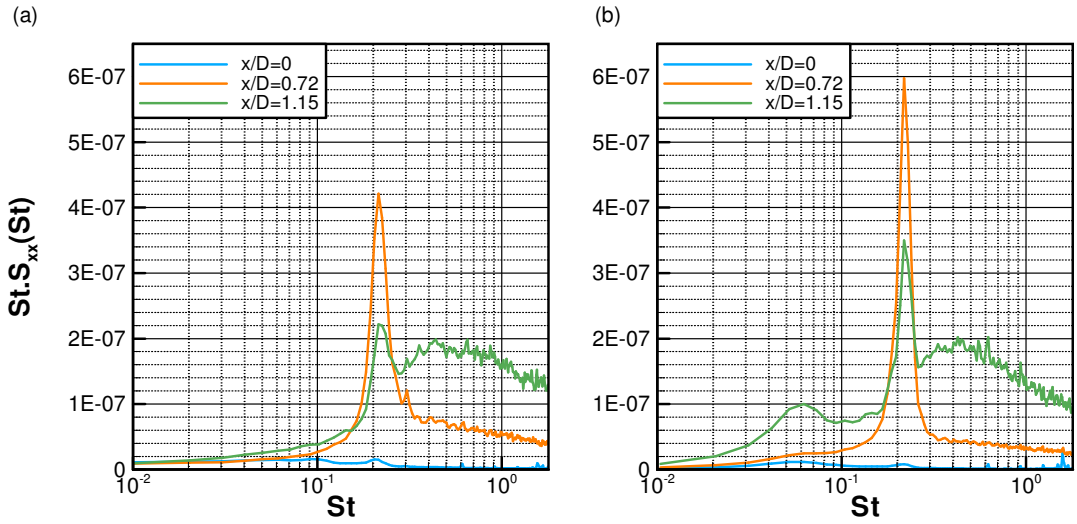

Figure 9. Spectra of the streamwise side load density CF_y for various positions on the rear-body, at M=0.7. (a): Nominal configuration. (b): Skirt configuration.

4. Conclusion

Extensive wall-pressure measurements have been performed on a long-rear afterbody configuration in the high subsonic and low supersonic regimes. The use of a short cylindrical serrated skirt as a buffeting reduction device was also considered.

The results obtained in the subsonic regime are in excellent agreement with those obtained in the past for slightly different Mach numbers [5], and confirm that the shear layer reattachment mainly accounts for the high level pressure fluctuations arising near the end of the rear-body. The azimuthal coherence

analysis shows that the vortex shedding is associated with a global destabilization of the near wake, due to a coherent m=1 mode, a result in agreement with local and global stability analysis performed on similar base flow configurations. This behaviour is not observed in the supersonic regime, where the pressure fluctuations are decorrelated.

By displacing downstream the separation point, the skirt prevents the shear layer from reattaching at the end of the rear-body, as seen in the nominal configuration. This results in a small reduction of the pressure and side loads fluctuation levels. However, we find no effect of the teeth, whereas the device was expected to modify the spatial organization of the separated flow region by enhancing small scale turbulence.

Acknowledgements

The authors thank the Centre National d'Etudes Spatiales (CNES) for financial support within the framework of the research and technology program ATAC (Aérodynamique des Tuyères et Arrière-Corps).

References

1. David, C. and Radulovic, S.: Prediction on buffet loads on the Ariane 5 Afterbody. In: *6th International Symposium on Launcher Technologies*, Germany (2005).
2. Délery, J. and Sirieix M., Base flow behind missiles. AGARD, Rept. LS-98 (1979).
3. Deprés, D., Analyse physique et modélisation des instationnarités dans les écoulements d'arrière-corps transsoniques. *Thèse de Doctorat*, ONERA (2003).
4. Deprés, D., Radulovic, S. and Lambaré, H.: Reduction of unsteady effects in afterbody transonic flows. In: *6th International Symposium on Launcher Technologies*, Germany (2005).
5. Deprés, D., Reijasse P. and Dussauge J.P., Analysis of unsteadiness in afterbody transonic flows. *AIAA Journal* ***42*** (2004) 2541–2550.
6. Eldred, K.M., Base pressure fluctuations. *Journal of the Acoustical Society of America* **33** (1961) 59–63.
7. Flodrops, J.P. and Desse J.M., Sillage d'un culot axisymétrique, Institut de Mécanique des Fluides de Lille, Rept. IMFL-85/19 (1985).
8. Mabey, D.G., Some measurements of base pressure fluctuations at subsonic and supersonic speeds. Aeronautical Research Council, ARC-CP-1204 (1972); also Royal Aircraft Establishment, Bedford, England. RAE-TR-70148, (1970).
9. Mabey, D.G., Pressure fluctuations caused by separated bubble flows at subsonic speeds. Royal Aircraft Establishment, Bedford, England. RAE-TR-71160, (1971).
11. Maury, B., Sondage de l'écoulement dans la zone décollée en aval d'une marche annulaire. ONERA, Meudon, Rept. ONERA-PV-2/0334-AY (1975).
12. Merz R.A., Subsonic base pressure fluctuations. *AIAA Journal* ***17*** (1979) 436–438.
13. Reijasse P. and Délery J., Investigation of the flow past the Ariane 5 launcher afterbody. *Journal of Spacecraft and Rockets* ***31*** (1994) 208–214.